EUROPEAN JOURNAL OF PURE AND APPLIED MATHEMATICS
2025, Vol. 18, Issue 4, Article Number 6896
ISSN 1307-5543 – ejpam.com
Published by New York Business Global

Mathematical Visualization of Fractal-Based Batik Designs

Khaleel Ahmad[1,2], Umar Ishtiaq[3], Mohammad Akram[4,*], Ioan-Lucian Popa[5,6]

[1] *Department of Mathematics, University of Management and Technology, Lahore 54770, Pakistan*
[2] *Center for Theoretical Physics, Khazar University, 41 Mehseti Str., Baku, AZ1096, Azerbaijan*
[3] *Office of Research Innovation and Commercialization, University of Management and Technology, Lahore 54770, Pakistan*
[4] *Department of Mathematics, Faculty of Science, Islamic University of Madinah, Madinah 42351, Saudi Arabia*
[5] *Department of Computing, Mathematics and Electronics, "1 Decembrie 1918" University of Alba Iulia, 510009 Alba Iulia, Romania*
[6] *Faculty of Mathematics and Computer Science, Transilvania University of Brasov, Iuliu Maniu Street 50, 500091 Brasov, Romania*

Abstract. In this manuscript, we use a rational-type mapping of a complex polynomial $S_c(z) = az^n + \frac{b}{z^m} + c$, where $a, b, c \in \mathbb{C}$ with $|a| > 1$, $m, n \in \mathbb{N}$ and $n > 1$, to generate Julia and Mandelbrot set fractals. We use the generalized viscosity approximation-type iterative scheme, extended with s-convexity for more control over the morphology of the resultant sets. Under this generalized viscosity approximation-type iterative scheme, a customized escape criterion is presented to precisely find orbit divergence. The structure, complexity, and symmetry of the produced fractals are investigated in relation to changing iterative parameters. We generate the Julia and Mandelbrot set fractals using MATLAB R2024a. Moreover, some Julia and Mandelbrot sets are created to generate Batik designs. This work not only broadens the theoretical underpinnings of fixed-point-based fractal generation but also links mathematical computation with useful applications in art and design.

2020 Mathematics Subject Classifications: 39B12, 37F10

Key Words and Phrases: Fractal geometry, iterative scheme, Mandelbrot set, Batik design, Julia set, fractals

*Corresponding author.
DOI: https://doi.org/10.29020/nybg.ejpam.v18i4.6896

Email addresses: s2023265011@umt.edu.pk (K. Ahmad), umarishtiaq@umt.edu.pk (U. Ishtiaq), akramkhan_20@rediffmail.com (M. Akram), lucian.popa@uab.ro (I.-L. Popa)

1. Introduction

Mathematical structures called fractals reveal unlimited complexity by means of self-similarity and recursion. These sophisticated objects are quite helpful for modeling irregular and nonlinear events across mathematics, physics, biology, and computer graphics. They capture forms too rough or fragmented to be explained by traditional Euclidean shapes, thus defying conventional geometry. In the study of dynamical systems, their recursive character and ability for modeling chaotic behavior make them especially useful. Fractals are not only mathematical curiosities, as Husain *et al.* [1] point out; they are ingrained in the patterns and processes of the natural world. Husain *et al.* [2] further underlined in a complementary survey that fractals continue to evolve as a topic of theoretical research and multidisciplinary innovation, stressing their various generative approaches and broad applications.

Two of the most famous examples of fractals resulting from intricate dynamics are the Julia and Mandelbrot sets. Their formation depends on the iterative behavior of complex-valued functions; they are well known for displaying a very sensitive dependence on initial conditions. Gaston Julia [3] and Pierre Fatou [4] investigated the iteration of rational functions, introducing the fundamental concepts for Julia sets. Benoit Mandelbrot [5] popularized these structures in the late twentieth century through his work on the Mandelbrot set, based on the iteration of the quadratic polynomial $z_{n+1} = z_n^2 + c$, $c \in \mathbb{C}$. His innovative visualizations exposed fractals as not only aesthetically beautiful but also mathematically profound.

Fixed-point iterative methods—mathematical processes used to approximate points that remain invariant under a given function—are largely responsible for the generation of Julia and Mandelbrot sets. Two of the earliest and most powerful methods in this field are the Mann iteration scheme [6], which introduced a mean-value iterative strategy to ensure convergence, and the Halpern iteration method [7], designed specifically for identifying fixed points of non-expansive mappings. More complex techniques evolved from these ideas. In particular, for nonlinear operators, Moudafi [8] presented the viscosity approximation method in 2000, a hybrid approach combining contraction mappings and iterative procedures to improve convergence. Since then, this approach has been a fundamental instrument for studying dynamical systems and fractals. Later, Mainge [9] extended this approach to quasi-nonexpansive mappings, thereby broadening its theoretical and practical applications.

Building on these iterative foundations, many researchers have investigated the dynamics of fractals using specific techniques. Romera *et al.* [10] advanced the study of fractal growth by exploring the exponential dynamics of complex functions using Picard iteration. Using an orbit-based method, Abbas *et al.* [11] developed new escape criteria for polynomials of different degrees, including quadratic, cubic, and higher-order forms. Particularly stressing affine and inverse transformations, Mork and Ulness [12] suggested incorporating Möbius transformations at each iteration step to produce visually rich Julia and Mandelbrot sets.

Recent work has extended fractal generation to trigonometric and transcendental

forms. While Qi *et al.* [13] and Hamada and Kharbat [14] investigated sine and cosine functions using nonstandard and Picard–Mann iterative frameworks, Prajapati *et al.* [15] applied the Mann iteration scheme to examine the behavior of entire transcendental functions. Using a four-step iterative process with s-convexity applied to cosine-type mappings, Tomar *et al.* [16] revealed intricate and highly structured fractal geometries. One important development in this field is the inclusion of s-convexity into iterative systems. Originally formalized by Pinheiro [17], s-convexity extends classical convexity and offers greater flexibility for examining convergence and stability in iterative processes. Rawat *et al.* [18] produced remarkable Julia and Mandelbrot sets from generalized rational mappings using the SP-iteration method enhanced with s-convexity.

Using Mann and Picard–Mann iterations, Tanveer *et al.* [19] investigated fractals of the form $z^p + \log(z)$, illustrating how parameter tuning affects structural complexity. Within the framework of extended Jungck–Noor orbits, Tassaddiq [20] proposed generalized escape criteria, thereby refining fractal generation techniques. Kumari *et al.* [21] built a unified viscosity-based framework to generate Julia sets, Mandelbrot sets, and biomorphs, while Kumari *et al.* [22] investigated the evolution of superior fractals under the Jungck–SP orbit with s-convexity. The application of fixed-point iteration methods for operator equation solving and the computation of zeros of maximal monotone mappings was discussed by Nandal *et al.* [23]. Emphasizing the dynamic interaction between iteration parameters and fractal geometry, Kumari *et al.* [24] studied the nonlinear behavior of viscosity-type iterations in Julia and Mandelbrot set generation. As Devaney [25] shows in his seminal work on chaotic dynamical systems, the sensitivity, recurrence, and complexity of fractals make them perfect objects for analyzing chaotic maps.

Underlining their rich visual and scientific impact, Peitgen *et al.* [26] demonstrated how fractals redefine our conception of order and chaos in both mathematical and physical systems. Araz and Çetin [27] used fractional derivatives in the sense of Caputo–Fabrizio, Caputo, and Atangana to discuss a modified COVID-19 model. Araz [28] introduced fractional integro-differential equations and discussed the existence and uniqueness of numerical schemes. Mekkaoui *et al.* [29] extended the predictor–corrector method to obtain numerical solutions of nonlinear differential equations. Uddin *et al.* [30] formulated a fixed-point theorem in controlled neutrosophic metric-like spaces with new control conditions guaranteeing the existence and uniqueness of fixed points in neutrosophic environments. Ishtiaq *et al.* [31] explored intuitionistic fuzzy N_b-metric spaces and derived corresponding fixed-point results with applications to nonlinear fractional differential equations. Ishtiaq *et al.* [32] proposed an extension of unique solution theorems in generalized neutrosophic cone metric spaces, introducing a more inclusive structure accommodating both neutrosophic and cone-based frameworks.

The paper is arranged in the following sections:

- Section 2, describes our work's theoretical underpinnings and prerequisites, together including the mathematical background and iterative structure.
- Section 3, we discuss the escape criteria for generalized viscosity approximation method, offers the suggested algorithms, and thorough graphical displays of the

produced fractals under several parameter values.

- In section 4, we compare our work with existing literature and section 5, is the conclusion and future work of our manuscript.

2. Preliminaries

In this section, we will discuss some definition like, Julia set, Mandelbrot set, s-convex combination, contraction mapping, and viscosity approximation method from existing literature.

Definition 1. *[3] Assume that S_c is a self-mapping on $\mathbb{C}$ and the collection of the set of points are*

$$F_{S_c} = \{z \in \mathbb{C} : \{|S_c^p(z)|\}_{p=0}^{\infty} \text{ is bounded}\}. \tag{1}$$

Then, the filled Julia set is denoted by F_{S_c}, that is the p^{th} iteration of S_c. If $n \geq 2$, then the Julia set refers to the boundary of the filled Julia set ∂F_{S_c}.

Definition 2. *[5] The Mandelbrot set M includes all parameter values β that are associated to the filled-in Julia set of $S_c(\varpi) = \varpi^2 + \beta$. That is,*

$$M = \{\varpi \in \mathbb{C} : \partial F_{S_c} \text{ is connected}\} \tag{2}$$

or

$$M = \{\varpi \in \mathbb{C} : |S_c(\varpi_n)| \to +\infty \text{ when } n \to +\infty\} \tag{3}$$

The element ϖ is a starting element in which $S_c(\varpi) = 0$.

Definition 3. *[17] Assume that $A \neq \varnothing$ has elements that are $z_1, z_2, \cdots, z_n$, and $s \in (0, 1]$. Then*

$$p_1^s z_1 + p_2^s z_2 + \cdots + p_n^s z_n, \tag{4}$$

is said to be s-convex combination, where $p_i \geq 0$ for $i \in \{1, 2, \cdots, n\}$ and $\sum_{k=1}^{n} p_i = 1$.

The process began with Moudafi's [8] 2000 pioneering work on the viscosity approximation method.

Definition 4. *Assume that $S : \mathbb{C} \to \mathbb{C}$ be a mapping of complex-valued polynomials. Give the following definition to the iterative sequence $\{z_i\}$:*

$$z_{i+1} = p_i g(z_i) + (1 - p_i) S(z_i), \quad i \geq 0, \tag{5}$$

where $z_0 \in \mathbb{C}$ is an arbitrary initial point, and $p_i \in (0, 1)$ is a real sequence governing the convex combination, $g : \mathbb{C} \to \mathbb{C}$ is a self-contraction mapping, or a function satisfying:

$$|g(z_1) - g(z_2)| < |z_1 - z_2| \quad \text{for all } z_1, z_2 \in \mathbb{C}. \tag{6}$$

An arbitrary point $z_0 \in \mathbb{C}$ starts the sequence $\{z_i\}$ and its development is controlled by a recursive relation intended to guarantee both stability and convergence. The iteration moves according to the recurrence formula shown as:

$$z_{i+1} = p_i g(z_i) + (1 - p_i) S_q z_i, \quad i \geq 0, \tag{7}$$

where g is a contraction mapping, S_c denotes the main nonlinear operator and $p_i, q \in (0, 1)$.

Kumari et al. [24] investigated a viscosity approximation-type iterative orbit initially proposed by Maange [9] that is:

$$\begin{cases} z_{i+1} = p_i g(z_i) + (1 - p_i) y_i, \\ y_i = q z_i + (1 - q) S_c(z_i), \quad i \geq 0, \end{cases} \tag{8}$$

starting from a point denominated by $z_0 \in \mathbb{C}$. Here $g : \mathbb{C} \to \mathbb{C}$ is a contraction mapping and S_c indicates a complex polynomial mapping. The complex function S_c is define as:

$$S_c(z) = z^n + bz + c, \tag{9}$$

where $n \geq 2$ and $b, c \in \mathbb{C}$. Furthermore, defined as $g(z) = az + \beta$, with $a, \beta \in \mathbb{C}$ and $|a| < 1$.

Definition 5. *Assume that c be a complex parameter in a complex set $\mathbb{C}$, and S_c be the generalized rational-type complex polynomial defined in equation 9. Using the viscosity approximation orbit provided in 8, define the iterative sequence $\{z_i\}$ with the initial condition $z_0 = 0$. Additionally, the viscosity Mandelbrot set M_c, denoted by*

$$M_c = \{c \in \mathbb{C} : |z_i| \nrightarrow \infty \text{ as } i \to \infty\}. \tag{10}$$

Accordingly, M_c consists of all complex parameters c for which the orbit $\{z_i\}$ remains bounded under the viscosity approximation iteration. For simplification, we use $p_i = p$, where $p \in (0, 1)$, throughout the manuscript.

3. Generalized Iterative Type Method

In this section, we present a generalized iterative approach for complex function $S_c(z) = az^n + \frac{b}{z^m} + c$, where $a, b, c \in \mathbb{C}$ with $|a| > 1, m, n \in \mathbb{N}$ with $n > 1$. By combining s-convexity and the structure of viscosity approximation schemes:

$$\begin{cases} y_i = q^s z_i + (1 - q)^s S_c(z_i), \\ w_i = p^s g(z_i) + (1 - p)^s y_i, \\ t_i = S_c(w_i), \\ z_{i+1} = S_c(t_i), \end{cases} \tag{11}$$

where $s \in (0,1], p, q \in (0,1), g$ is a contraction mapping on $\mathbb{C}$, $z_0 \in \mathbb{C}$ is the starting point, and S_c is a complex polynomial. The generalized rational type complex polynomial is defined as:

$$S_c(z) = az^n + \frac{b}{z^m} + c, \tag{12}$$

where $a, b, c \in \mathbb{C}$ with $|a| > 1, m, n \in \mathbb{N}$ with $n > 1$, and complex contraction $g(z) = \alpha z + \beta$, where $\alpha, \beta \in \mathbb{C}$ with $|\alpha| < 1$.

3.1 Escape Criterion

Many approaches have been developed in the part of fractal geometry for the generation and analysis of intricate fractals including iterated function systems, distance estimator methods, escape-time algorithms, and potential functions [26]. Among these, the escape-time algorithm stays among the most important and often used techniques. Fundamentally, the escape-time criterion offers a basic guidance for deciding whether the orbit of an initial point under a given complex function stays limited or diverges to infinity. Since it controls the iterative behavior of intricate mappings across the complex plane, this classification forms at the core of fractal generation.

In this research we propose a thorough escape criterion designed especially for producing Julia and Mandelbrot sets under viscosity approximation-type orbits extended with s-convexity. The formulation considers the interaction of complicated dynamics including contraction mappings and a generalized rational-type complex polynomial. Designed to robustly classify complicated points in the framework of the proposed iterative scheme, this escape condition provides a computationally efficient and mathematically sound method for fractal generation.

Theorem 1. *Let $S_c(z) = az^n + \frac{b}{z^m} + c$ be a generalized rational-type complex polynomial of degree n, and $g(z) = \alpha z + \beta$ a complex contraction, where $\alpha, \beta \in \mathbb{C}$ with $|\alpha| < 1$. Assume that:*

$$|z_0| \geq \max\{|c|, |\beta|\} > \left(\frac{2 + sp}{(1 - sp)(1 - sq)(|\alpha| - 1)}\right)^{\frac{1}{(n-1)}}, \tag{13}$$

and $|z_0| \geq |b|^{1/(n+m)}$, where $a, b, c \in \mathbb{C}$ with $|a| > 1, m, n \in \mathbb{N}$ with $n > 1$. Define a sequence (11) Then, $|z_i| \to \infty$ as $i \to \infty$.

Proof. Consider the sequence defined in (11),

$$|y_0| = |q^s z_0 + (1 - q)^s S_c(z_0)| = |q^s z_0 + (1 - q)^s (az_0^n + \frac{b}{z_0^m} + z)|.$$

By utilizing the binomial expansion of $(1 - q)^s$ up to the linear terms of q and considering the inequality $q^s \geq sq$, we obtain

$$|y_0| \geq |sqz_0 + (1 - sq)(az_0^n + \frac{b}{z_0^m} + c)|$$

$$\geq |(1-sq)(az_0^n + \frac{b}{z_0^m} + c)| - sq|z_0|$$

$$\geq (1-sq)|(az_0^n + c)| - (1-sq)|\frac{b}{z_0^m}| - sq|z_0|.$$

By our assumption $|z_0| \geq \max\{|c|, |\beta|\}$, it follows that $|z_0| \geq |c|$. Furthermore, from the assumption $|z_0| \geq |b|^{1/(n+m)}$, we get

$$|y_0| \geq (1-sq)|az_0^n| - (1-sq)|(z_0^{n+m}/z_0^m)| - (1-sq)|z_0| - sq|z_0| = (1-sq)|az_0^n| - (1-sq)|z_0^n| - |z_0|,$$

$$|y_0| \geq |z_0|[(1-sq)(|a|-1)|z_0^{n-1}| - 1]. \tag{14}$$

Using (11), the binomial expansion of $(1-p)^s$ up to the first-order terms of p, and the inequality $p^s \geq sp$, we arrive at

$$|w_0| \geq |sp(az_0 + \beta) + (1-sp)y_0|.$$

This leads us to

$$|w_0| \geq (1-sp)|y_0| - sp|\alpha z_0| - sp|z_0| > (1-sp)|y_0| - sp|z_0| - sp|z_0|,$$

as $|z_0| \geq \max\{|c|, |\beta|\}$. Using (14), we obtain

$$|w_0| > |z_0|[(1-sp)(1-sq)(|a|-1)|z_0^{n-1}| - sp - 1].$$

Because

$$|z_0| > \left(\frac{2+sp}{(1-sp)(1-sq)(|a|-1)}\right)^{1/(n-1)}.$$

Then, we have

$$(1-sp)(1-sq)(|a|-1)|z_0^{n-1}| - sp - 1 > 1.$$

Thus, there exists a positive real number μ such that

$$(1-sp)(1-sq)(|a|-1)|z_0^{n-1}| - sp - 1 > \mu + 1.$$

Hence, $|t_0| = S_C(w_0) > |w_0|$ and $|z_1| > |t_0| > |w_0| > |y_0| > |z_0|$, and $|z_1| > (\mu+1)|z_0|$. With $|z_1|$ being greater than $|z_0|$, continuously this process, there exist a real number $\mu > 0$, such that $|z_i| > (\mu+1)^i|z_0|$. Hence, $|z_i| \to \infty$ as $i \to \infty$.

We refine the above theorem with the following corollaries.

Corollary 1. *Let* $|z_0| \geq \max\{|c|, |\beta|, |b|^{1/(n+m)}, ((2+sp)/(1-sp)(1-sq)(|a|-1))^{1/(n-1)}\} = R$, *where* $s \in (0,1]$ *and* $0 < p, q < 1$. *Then, there exists* $\mu > 0$ *such that* $|z_i| > (1+\mu)^i|z_0|$, *and we have* $|z_i| \to \infty$ *as* $i \to \infty$.

Corollary 2. *Suppose that* $|z_j| \geq \max\{|c|, |\beta|, |b|^{1/(n+m)}, ((2+sp)/(1-sp)(1-sq)(|a|-1))^{1/(n-1)}\} = R$, *for some* $j \geq 0$, *where* $s \in (0,1], 0 < p, q < 1, a, b, c \in \mathbb{C}$ *with* $|a| > 1$, *and* $m, n \in \mathbb{N}$ *with* $n > 1$. *Then, there exists* $\mu > 0$ *such that* $|z_{i+j}| > (1+\mu)^i|z_j|$, *and we have* $|z_j| \to \infty$ *as* $i \to \infty$.

3.2 Algorithms

Corresponding to an nth-degree generalized rational-type complex polynomial $S_c(z) = az^n + \frac{b}{z^m} + c$, where $a, b, c \in \mathbb{C}$ with $|a| > 1, m, n \in \mathbb{N}, n > 1$, Corollaries 1 and 2 offer a convenient framework for the construction of both Julia and Mandelbrot sets. A circle of radius R in the complex plane defines this threshold where is defined as

$$R = \max\left\{|c|, |\beta|, |b|^{\frac{1}{n+m}}, \left(\frac{2+sp}{(1-sp)(1-sq)(|a|-1)}\right)^{\frac{1}{n-1}}\right\}.$$

The parameter, R is the escape radius, beyond which the sequence veers off to infinity. The orbit is regarded unbounded if the modulus $|z_i| > R$ for any i; the point z_0 is therefore excluded from the set.

Algorithm 1: Generation of Julia set fractals

Require: $S_c(z) = az^n + \frac{b}{z^m} + c$, where $a, b, c \in \mathbb{C}$ with $|a| > 1$, $m, n \in \mathbb{N}$ and $n > 1$; $A \subset \mathbb{C}$ – the region from which the set is drawn; the maximum number of iterations is denoted by K_1; $p, q \in (0, 1)$, and $s \in (0, 1]$ are the parameters for the new iterative method; $g(z) = \alpha z + \beta$, where $\alpha, \beta \in \mathbb{C}$ and $|\alpha| < 1$; colormap $[0..K_1]$ with $K_1 + 1$ colors.

Ensure: Julia set for A.

Steps:

$R = \max\left\{|c|, |\beta|, |b|^{1/(n+m)}, \left(\frac{2+sp}{(1-sp)(1-sq)(|a|-1)}\right)^{1/(n-1)}\right\}$;

for $z_0 \in A$ **do**
  $i = 0$;
  while $|z_i| < R$ **and** $i < K_1$ **do**
    $y_i = q^s z_i + (1-q)^s S_c(z_i)$;
    $w_i = p^s g(z_i) + (1-p)^s y_i$;
    $t_i = S_c(w_i)$;
    $z_{i+1} = S_c(t_i)$;
    $i = i + 1$;
  end while
  color z_0 with colormap$[i]$;
end for

Algorithm 2: Generation of Mandelbrot set fractals

Require: $S_c(z) = az^n + \frac{b}{z^m} + c$, where $a, b, c \in \mathbb{C}$ with $|a| > 1$, $m, n \in \mathbb{N}$ and $n > 1$; $A \subset \mathbb{C}$ – the area; K_1 – the maximum number of iterations; $p, q, s \in (0, 1)$ are the parameters for the new iterative method; $g(z) = \alpha z + \beta$, where $\alpha, \beta \in \mathbb{C}$ and $|\alpha| < 1$; colormap $[0..K_1]$ with $K_1 + 1$ colors.

Ensure: Mandelbrot set for area A.

Steps:

for $c \in A$ **do**

$R = \max\left\{|c|, |\beta|, |b|^{1/(n+m)}, \left(\frac{2+sp}{(1-sp)(1-sq)(|a|-1)}\right)^{1/(n-1)}\right\}$;

$i = 0$;

$z_0 = c$;

while $|z_i| < R$ **and** $i < K_1$ **do**

$y_i = qz_i + (1-q)S_c(z_i)$;

$w_i = p^s g(z_i) + (1-p)^s y_i$;

$t_i = S_c(w_i)$;

$z_{i+1} = S_c(t_i)$;

$i = i + 1$;

end while

color c with colormap$[i]$;

end for

We use an image resolution of 400×400 pixels for the numerical simulations to guarantee a computationally efficient but visually instructive rendering of the fractals. With a total of 50 iterations ($K = 100$), the Julia set is computed allowing for a finer approximation of the complex boundary structures and subtle details unique of Julia fractals. In this context, a higher iteration count is required to faithfully depict the intricate dynamics and self-similarity intrinsic in the orbit behavior of points under the selected mapping.

By contrast, the Mandelbrot set is produced in thirty iterations ($K = 100$). A rather low iteration threshold is usually enough to separate members from non-members since the Mandelbrot set's point classification is intrinsically binary determining whether the orbit remains limited or escapes to infinity. This low iteration count provides a good compromise between computational speed and the capacity to record the main structural elements of the Mandelbrot set.

Example for the Julia set

We investigate the Julia set behavior produced under a generalized rational-type mapping using orbits extended with s-convexity inside the framework of the generalized viscosity approximation method. The aim is to investigate, especially the complex coefficient β, how geometric and topological properties of the produced fractals vary with changes in input parameters.

Figure 1 shows the visual development of the Julia set under this generalized mapping. In this experiment, $n = 2, m = 9, a = 1 - 0.05i, b = 0.6 - 0.3i, \alpha = -0.99, p = 0.85, q = 0.95, s = 0.99$. We methodically change the parameter β over six different complex values to see how it affects the Julia set's complexity and form. These variations let us investigate the sensitivity of the iteration process to fluctuations in β.

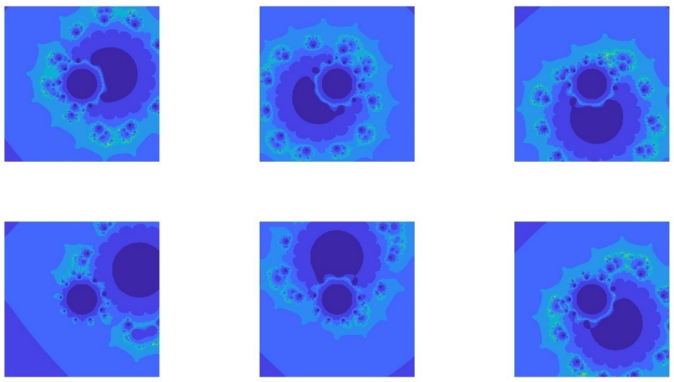

Figure 1: depicts the Julia set fractals for different values of the parameter β.

Figure 1 shows the Julia set fractal structure produced by a generalized viscosity approximation process under various parameter settings, primarily due to changes in the parameter β. Although all subplots share a similar color scheme—mostly dominated by blue and cyan tones—the internal structures exhibit clear variations in shape, complexity, and fractal pattern distribution. The other parameters n, m, a, b, c, s, p, q, and α are kept constant. The values of all parameters are listed in Table 1.

Table 1: Variation of the parameter β.

n	**m**	**a**	**b**	**c**	**s**	**p**	**q**	$\boldsymbol{\alpha}$	$\boldsymbol{\beta}$
2	9	$1 - 0.05i$	$0.6 + 0.3i$	$0.03 + 0.07i$	0.99	0.85	0.95	-0.99	$0.6 - 0.2i$
2	9	$1 - 0.05i$	$0.6 + 0.3i$	$0.03 + 0.07i$	0.99	0.85	0.95	-0.99	$-0.4 + 0.3i$
2	9	$1 - 0.05i$	$0.6 + 0.3i$	$0.03 + 0.07i$	0.99	0.85	0.95	-0.99	$0.1 + 0.7i$
2	9	$1 - 0.05i$	$0.6 + 0.3i$	$0.03 + 0.07i$	0.99	0.85	0.95	-0.99	$1.2 - 0.6i$
2	9	$1 - 0.05i$	$0.6 + 0.3i$	$0.03 + 0.07i$	0.99	0.85	0.95	-0.99	$-0.9i$
2	9	$1 - 0.05i$	$0.6 + 0.3i$	$0.03 + 0.07i$	0.99	0.85	0.95	-0.99	$0.5 - 0.5i$

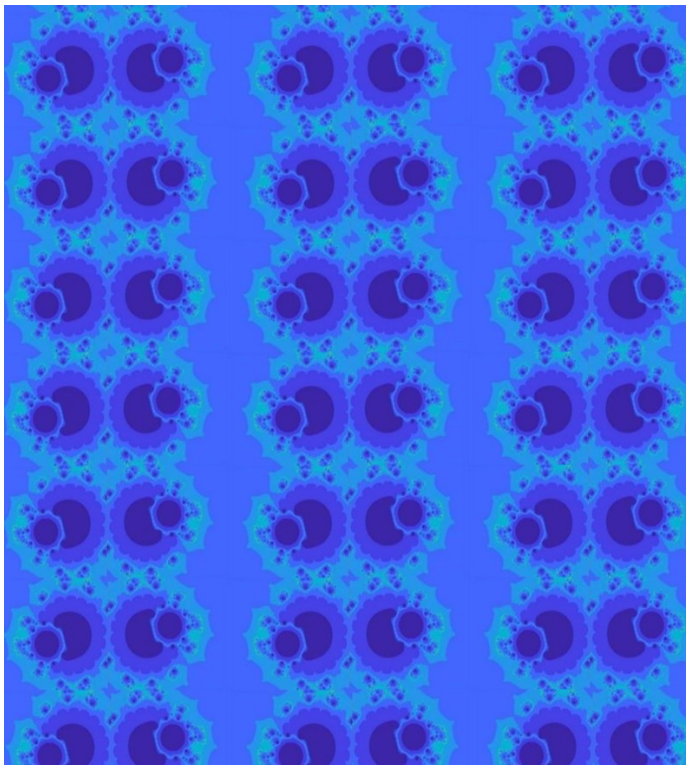

Figure 2: depicts the Batik design obtained by using the second subsection of Figure 1.

Figure 2, features a regular grid arrangement of repeated identical Julia sets set in a Batik pattern. Every fractal tile consists of a central bulbous form surrounded by symmetric, scalloped edges, and smaller satellite forms.

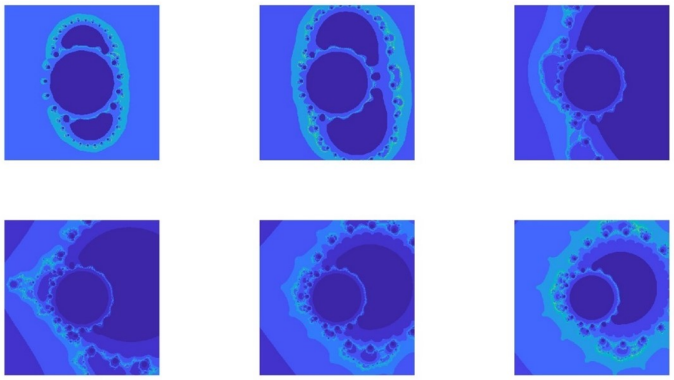

Figure 3: depicts the Julia fractals for different values of s.

Figure 3 shows six different Julia set fractals, each matching different parameter configurations, probably varying the parameter s while the other parameters are fixed. Two main lobes or bulbous areas define a bifurcated structure in the dynamical behavior of the

chosen function and are a fundamental characteristic of all images. Suggesting a balanced contribution from real and imaginary components of the complex parameters, the left and center images in the top row show highly symmetrical "double-lobed" forms with circular inner voids and fine boundary structures.

Table 2: variation of the parameter s.

n	**m**	**a**	**b**	**c**	**s**	**p**	**q**	$\boldsymbol{\alpha}$	$\boldsymbol{\beta}$
2	15	$1-0.05i$	$0.6+0.3i$	$0.03+0.07i$	0.1	0.85	0.95	-0.99	$0.6-0.2i$
2	15	$1-0.05i$	$0.6+0.3i$	$0.03+0.07i$	0.2	0.85	0.95	-0.99	$0.6-0.2i$
2	15	$1-0.05i$	$0.6+0.3i$	$0.03+0.07i$	0.4	0.85	0.95	-0.99	$0.6-0.2i$
2	15	$1-0.05i$	$0.6+0.3i$	$0.03+0.07i$	0.6	0.85	0.95	-0.99	$0.6-0.2i$
2	15	$1-0.05i$	$0.6+0.3i$	$0.03+0.07i$	0.8	0.85	0.95	-0.99	$0.6-0.2i$
2	15	$1-0.05i$	$0.6+0.3i$	$0.03+0.07i$	0.99	0.85	0.95	-0.99	$0.6-0.2i$

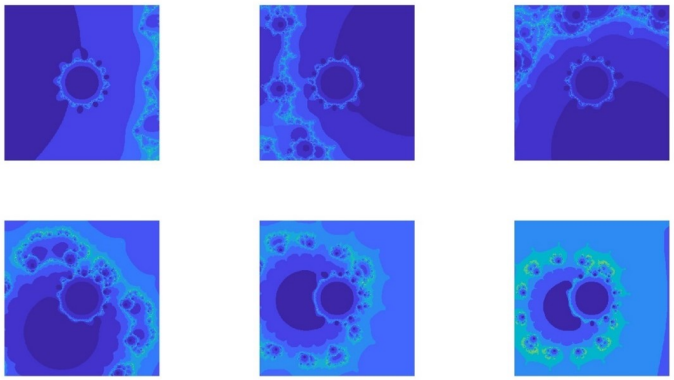

Figure 4: depict the behavior of Julia set fractal for different values of the parameter α.

Each of the subsections of the Julia set fractals shown in Figure 4 has a different geometric structure shaped by varying the parameter α, while the other parameters n, m, a, b, c, s, p, q, and β are fixed. Though their color palette consists regularly of blue to cyan with traces of green, each subplot exposes different morphologies in the core and boundary areas.

Table 3: Variation of the parameter .

n	**m**	**a**	**b**	**c**	**s**	**p**	**q**	$\boldsymbol{\alpha}$	$\boldsymbol{\beta}$
2	10	$1-0.05i$	$0.6+0.3i$	$0.03+0.07i$	0.99	0.85	0.95	$-0.1i$	$0.6-0.2i$
2	10	$1-0.05i$	$0.6+0.3i$	$0.03+0.07i$	0.99	0.85	0.95	0.5	$0.6-0.2i$
2	10	$1-0.05i$	$0.6+0.3i$	$0.03+0.07i$	0.99	0.85	0.95	$-0.2+0.3i$	$0.6-0.2i$
2	10	$1-0.05i$	$0.6+0.3i$	$0.03+0.07i$	0.99	0.85	0.95	$0.3+0.4i$	$0.6-0.2i$
2	10	$1-0.05i$	$0.6+0.3i$	$0.03+0.07i$	0.99	0.85	0.95	$0.6-0.2i$	$0.6-0.2i$
2	10	$1-0.05i$	$0.6+0.3i$	$0.03+0.07i$	0.99	0.85	0.95	0.8	$0.6-0.2i$

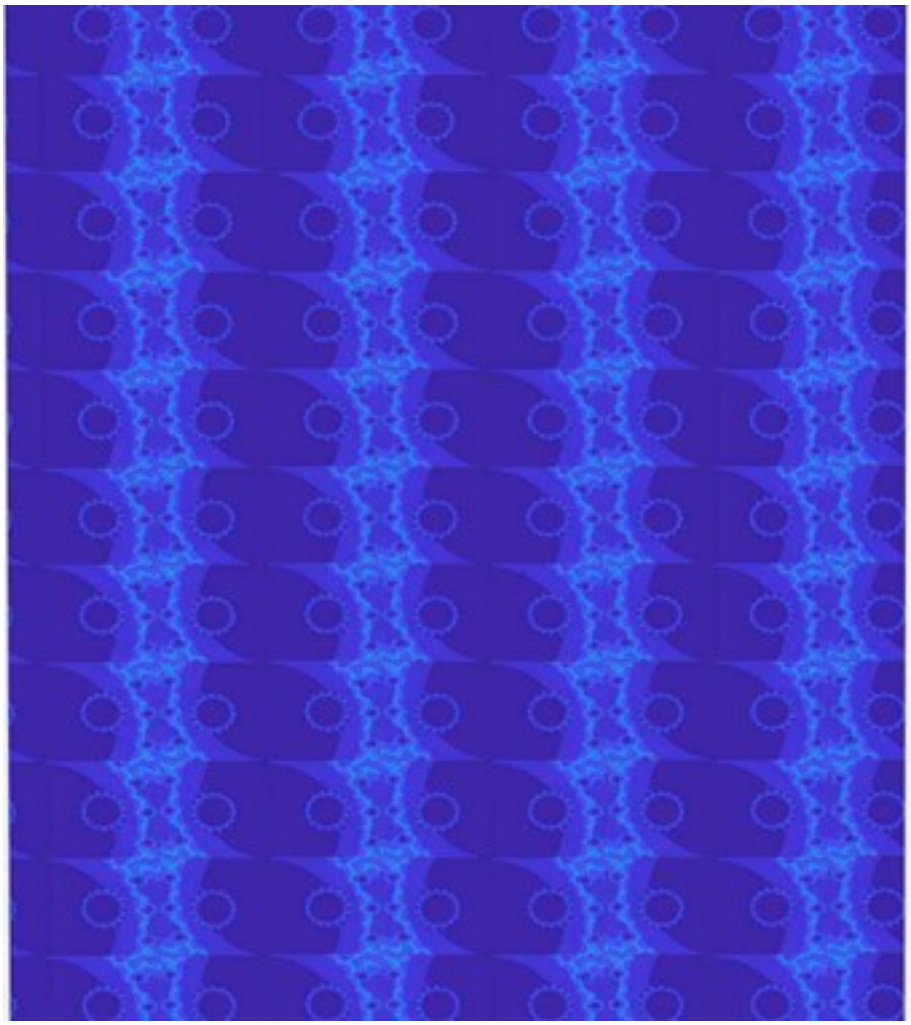

Figure 5: depicts the Batik design obtained by using the third subsection of Figure 4.

Figure 6: depicts the Batik design obtained by using the third subsection of Figure 4.

Use third subsection of Figure 4, forms repeatedly to create a decorative and symmetrical design.

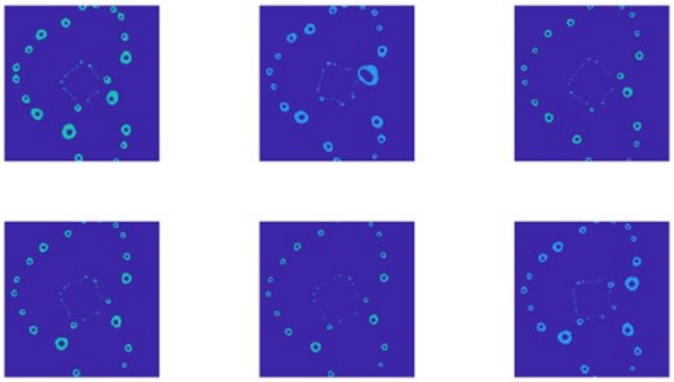

Figure 7: depicts the Julia set fractals for different values of the parameter b.

Figure 7 shows the behavior of Julia set fractals obtained using the generalized viscosity approximation process with variation of the parameter b while the other parameters $n, m, a, c, s, p, q, \alpha$, and β are fixed.

Table 4: Variation of the parameter b.

n	**m**	**a**	**b**	**c**	**s**	**p**	**q**	$\boldsymbol{\alpha}$	$\boldsymbol{\beta}$
3	2	$2+0.5i$	$0.3+0.3i$	$-0.3-0.7i$	0.9	0.7	0.8	0.5	$0.6+0.2i$
3	2	$2+0.5i$	$-0.5i$	$-0.3-0.7i$	0.9	0.7	0.8	0.5	$0.6+0.2i$
3	2	$2+0.5i$	0.9	$-0.3-0.7i$	0.9	0.7	0.8	0.5	$0.6+0.2i$
3	2	$2+0.5i$	$-0.2-0.7i$	$-0.3-0.7i$	0.9	0.7	0.8	0.5	$0.6+0.2i$
3	2	$2+0.5i$	$1.1i$	$-0.3-0.7i$	0.9	0.7	0.8	0.5	$0.6+0.2i$
3	2	$2+0.5i$	-0.6	$-0.3-0.7i$	0.9	0.7	0.8	0.5	$0.6+0.2i$

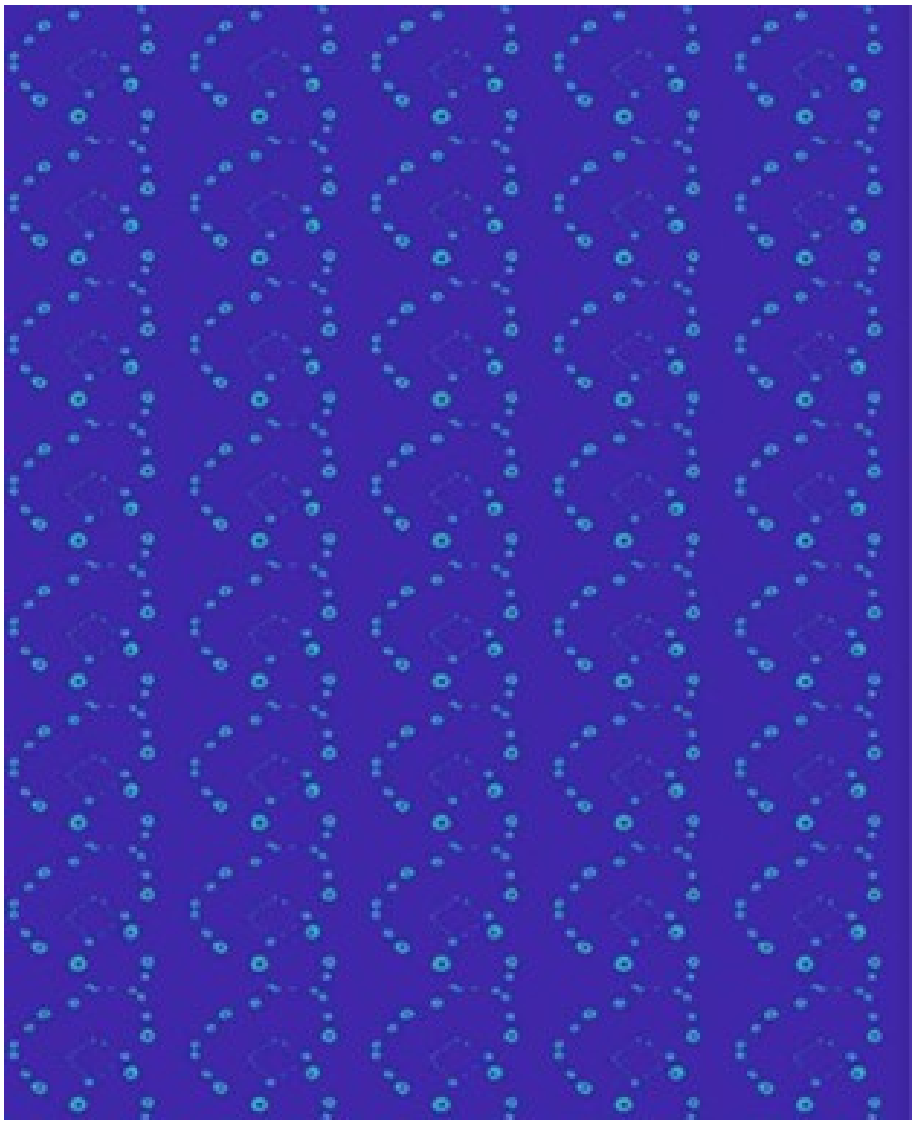

Figure 8: depicts the Batik design obtained by using the sixth subsection of Figure 7.

The Figure 8, presented here is a symmetric, horizontally and vertically replicated fractal design containing discrete, round Julia set islands systemically placed within a geometric design.

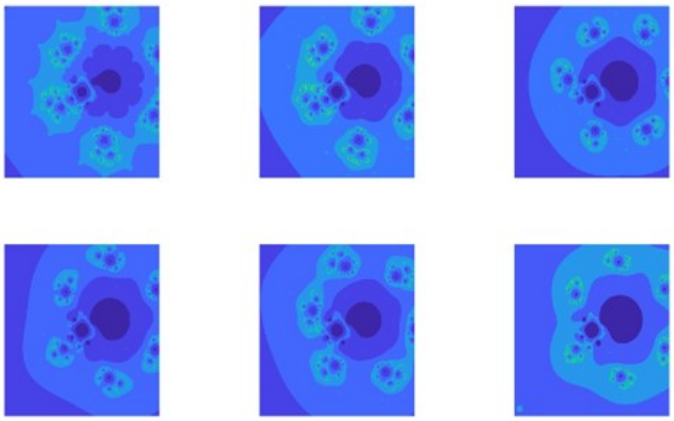

Figure 9: depict the Julia set fractal for different values of a.

Each Julia set fractal generated in Figure 9 is obtained by varying the parameter a while keeping the other parameters constant. The values of the parameters $n, m, a, b, c, s, p, q, \alpha$, and β are shown in Table 5.

Table 5: Variation of the parameter a.

n	**m**	**a**	**b**	**c**	**s**	**p**	**q**	$\boldsymbol{\alpha}$	$\boldsymbol{\beta}$
3	2	$0.3+0.3i$	$2+0.5i$	$2+0.5i$	0.9	0.7	0.8	0.5	$0.6+0.2i$
3	2	$-0.5i$	$2+0.5i$	$2+0.5i$	0.9	0.7	0.8	0.5	$0.6+0.2i$
3	2	0.9	$2+0.5i$	$2+0.5i$	0.9	0.7	0.8	0.5	$0.6+0.2i$
3	2	$-0.2-0.7i$	$2+0.5i$	$2+0.5i$	0.9	0.7	0.8	0.5	$0.6+0.2i$
3	2	$1.1i$	$2+0.5i$	$2+0.5i$	0.9	0.7	0.8	0.5	$0.6+0.2i$
3	2	-0.6	$2+0.5i$	$2+0.5i$	0.9	0.7	0.8	0.5	$0.6+0.2i$

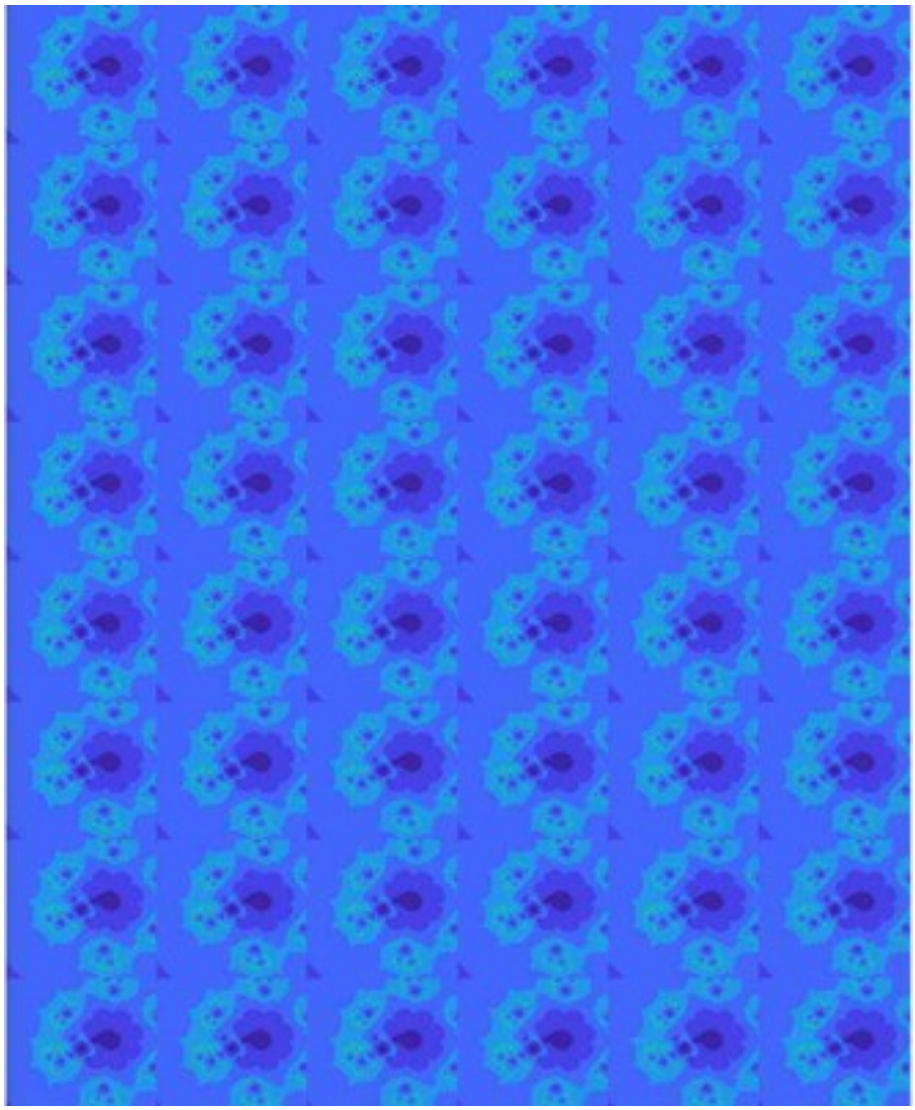

Figure 10: depicts the Batik design obtained by using the first subsection of Figure 9.

A visually striking texture is produced by the uniform tiling of identical Julia fractal patterns set methodically over the whole visual plane shown in Figure 10.

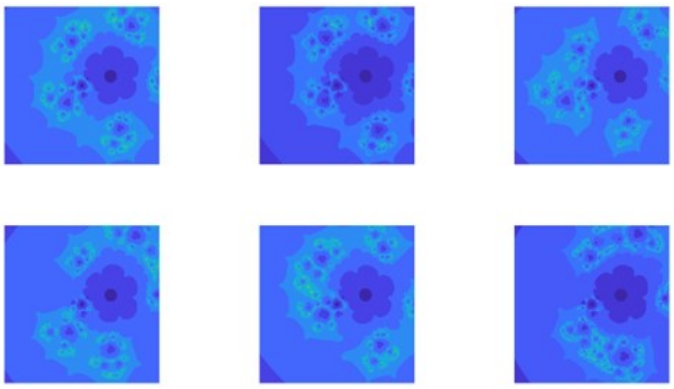

Figure 11: depict the Julia set fractal for different values of c.

Each of the Julia set fractals shown in Figure 11, shows minute changes resulting from change in fractal parameter c. Every subplot has a centrally located multi-lobed core surrounded by uniquely formed fractal "petals." The fractals show their sensitivity to parameter variations mostly in the number, position, and complex details of these periphery structures. While the bottom row reveals more asymmetrical forms with petals appearing broken or rotated, indicating a change in the iterative conditions or parameters, the top row shows symmetrical configurations with clearly defined central flower-like forms.

Table 6: Variation of the parameter c.

n	**m**	**a**	**b**	**c**	**s**	**p**	**q**	$\boldsymbol{\alpha}$	$\boldsymbol{\beta}$
2	4	$1-0.05i$	$0.6+0.3i$	$0.03+0.07i$	0.99	0.85	0.95	-0.99	$0.6-0.2i$
2	4	$1-0.05i$	$0.6+0.3i$	$0.1-0.2i$	0.99	0.85	0.95	-0.99	$0.6-0.2i$
2	4	$1-0.05i$	$0.6+0.3i$	$-0.6+0.4i$	0.99	0.85	0.95	-0.99	$0.6-0.2i$
2	4	$1-0.05i$	$0.6+0.3i$	$0.5+0.6i$	0.99	0.85	0.95	-0.99	$0.6-0.2i$
2	4	$1-0.05i$	$0.6+0.3i$	$-0.2-0.3i$	0.99	0.85	0.95	-0.99	$0.6-0.2i$
2	4	$1-0.05i$	$0.6+0.3i$	$0.8+0.2i$	0.99	0.85	0.95	-0.99	$0.6-0.2i$

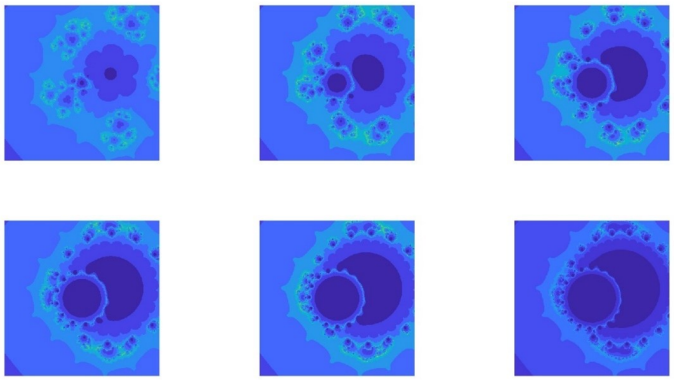

Figure 12: depict the Julia set fractal for different values of m.

Figure 12 shows the behavior of the Julia set fractals for the variation of the parameter m while the other parameters are constant. The values of m are 3, 6, 9, 12, 15, and 18 are shown in Table 7.

Table 7: Variation of the parameter m.

n	**m**	**a**	**b**	**c**	**s**	**p**	**q**	$\boldsymbol{\alpha}$	$\boldsymbol{\beta}$
2	3	$1-0.05i$	$0.6+0.3i$	$0.03+0.07i$	0.99	0.85	0.95	-0.99	$0.6-0.2i$
2	6	$1-0.05i$	$0.6+0.3i$	$0.03+0.07i$	0.99	0.85	0.95	-0.99	$0.6-0.2i$
2	9	$1-0.05i$	$0.6+0.3i$	$0.03+0.07i$	0.99	0.85	0.95	-0.99	$0.6-0.2i$
2	12	$1-0.05i$	$0.6+0.3i$	$0.03+0.07i$	0.99	0.85	0.95	-0.99	$0.6-0.2i$
2	15	$1-0.05i$	$0.6+0.3i$	$0.03+0.07i$	0.99	0.85	0.95	-0.99	$0.6-0.2i$
2	18	$1-0.05i$	$0.6+0.3i$	$0.03+0.07i$	0.99	0.85	0.95	-0.99	$0.6-0.2i$

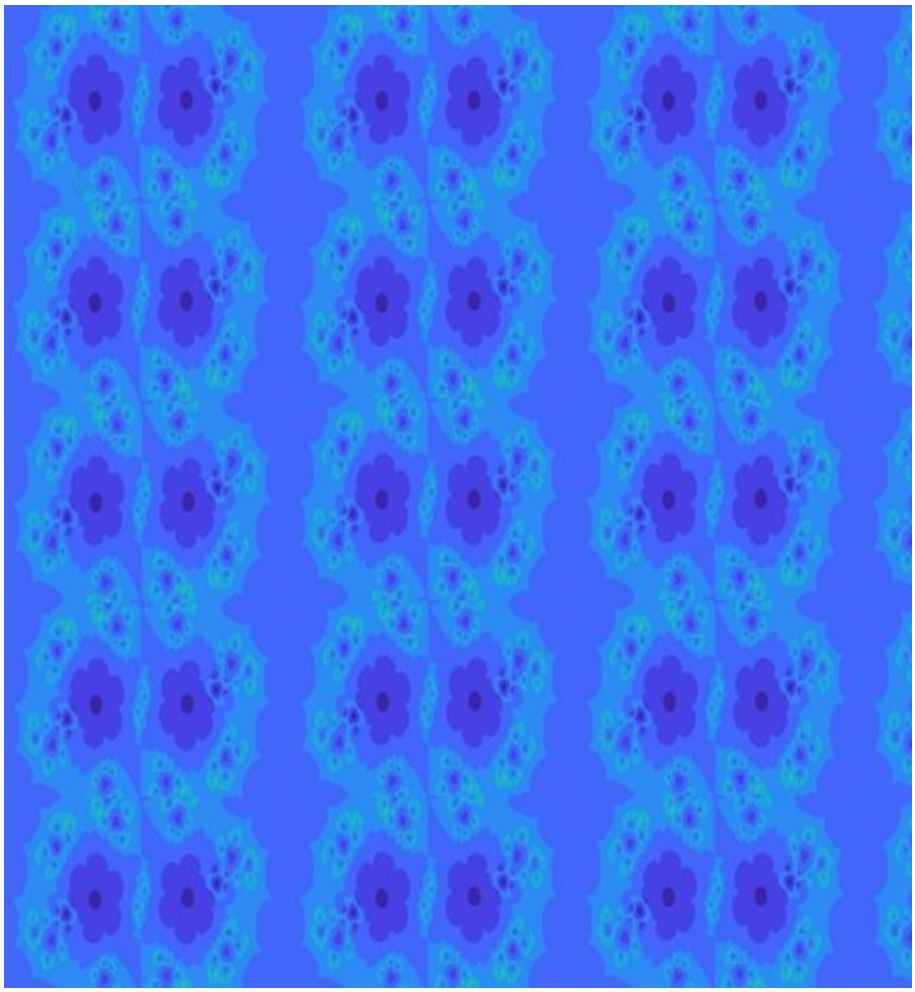

Figure 13: depicts the Batik design obtained by using the first subsection of Figure 12.

Figure 14: depicts the Batik design obtained by using the first subsection of Figure 12.

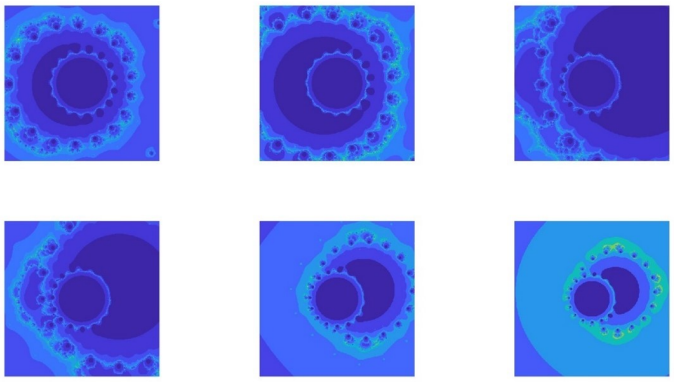

Figure 15: depict the Julia set fractal for different values of p.

Figure 15 shows the behavior of the Julia set fractals obtained using the generalized viscosity approximation process with variation of the parameter p, while the other parameters $n, m, a, b, c, s, q, \alpha$, and β remain fixed.

Table 8: Variation of the parameter p.

n	**m**	**a**	**b**	**c**	**s**	**p**	**q**	$\boldsymbol{\alpha}$	$\boldsymbol{\beta}$
2	15	$1-0.05i$	$0.6+0.3i$	$0.03+0.07i$	0.99	0.15	0.95	-0.99	$0.6-0.2i$
2	15	$1-0.05i$	$0.6+0.3i$	$0.03+0.07i$	0.99	0.20	0.95	-0.99	$0.6-0.2i$
2	15	$1-0.05i$	$0.6+0.3i$	$0.03+0.07i$	0.99	0.70	0.95	-0.99	$0.6-0.2i$
2	15	$1-0.05i$	$0.6+0.3i$	$0.03+0.07i$	0.99	0.75	0.95	-0.99	$0.6-0.2i$
2	15	$1-0.05i$	$0.6+0.3i$	$0.03+0.07i$	0.99	0.90	0.95	-0.99	$0.6-0.2i$
2	15	$1-0.05i$	$0.6+0.3i$	$0.03+0.07i$	0.99	0.99	0.95	-0.99	$0.6-0.2i$

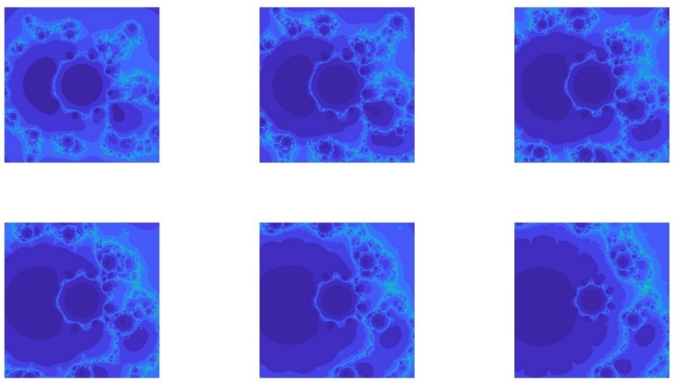

Figure 16: depict the Julia set fractal for different values of q.

Starting with large bulbous central structures surrounded by smaller connected areas,

the fractal patterns in the first subsection of Figure 16 show rounded, smooth boundaries.

Table 9: variation of the parameter q.

n	**m**	**a**	**b**	**c**	**s**	**p**	**q**	$\boldsymbol{\alpha}$	$\boldsymbol{\beta}$
2	8	$1-0.05i$	$-0.6+0.3i$	$0.03+0.07i$	0.99	0.85	0.20	$-0.6-0.2i$	$0.6-0.2i$
2	8	$1-0.05i$	$-0.6+0.3i$	$0.03+0.07i$	0.99	0.85	0.40	$-0.6-0.2i$	$0.6-0.2i$
2	8	$1-0.05i$	$-0.6+0.3i$	$0.03+0.07i$	0.99	0.85	0.60	$-0.6-0.2i$	$0.6-0.2i$
2	8	$1-0.05i$	$-0.6+0.3i$	$0.03+0.07i$	0.99	0.85	0.75	$-0.6-0.2i$	$0.6-0.2i$
2	8	$1-0.05i$	$-0.6+0.3i$	$0.03+0.07i$	0.99	0.85	0.90	$-0.6-0.2i$	$0.6-0.2i$
2	8	$1-0.05i$	$-0.6+0.3i$	$0.03+0.07i$	0.99	0.85	0.99	$-0.6-0.2i$	$0.6-0.2i$

3.4 Fractals for Mandelbrot Set

In the following section, we investigate the Mandelbrot set for a generalized rational-type condition by using orbits extended with s-convexity under the generalized viscosity approximation method for different input parameters.

Seeing Figures 21 and 22 makes it clear that the form of the set is strongly influenced by the parameters p and q. The set expands and changes in form as both parameters increase. Furthermore, one finds interesting axial symmetry in the produced sets.

Examining Figures 17–25, it is evident that changing the parameters—particularly p, q, s, α, and β—has a significant effect on the form of the resulting set. The set grows in size as these parameters increase and simultaneously adopts a more varied exploration, thus compromising some of its finer nuances.

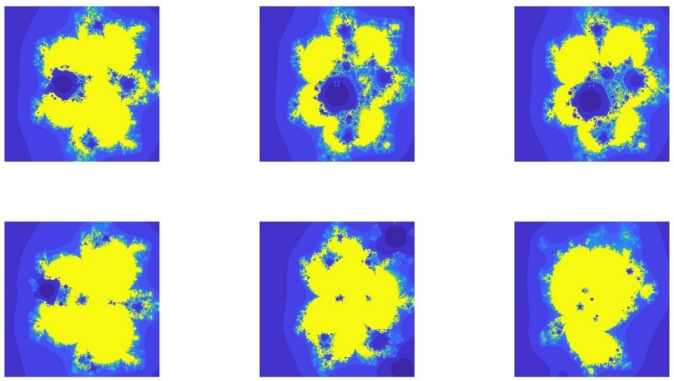

Figure 17: depict Mandelbrot set fractal for different values of β.

In Figure 17, we observe the Mandelbrot set fractal behavior for different values of the parameter β. From left to right, the fractals in the top row gradually become more complex and irregular. With smoother boundaries and fewer smaller peripheral clusters, the leftmost subplot displays large, compact yellow structures that dominate the visualization.

Table 10: variation of the parameter β.

n	**m**	**a**	**b**	**s**	**p**	**q**	$\boldsymbol{\alpha}$	$\boldsymbol{\beta}$
2	4	$0.006 - 0.001i$	$0.000045i$	0.99	0.85	0.80	$-0.006 - 0.001i$	$0.1 - 0.003i$
2	4	$0.006 - 0.001i$	$0.000045i$	0.99	0.85	0.80	$-0.006 - 0.001i$	$-0.05i$
2	4	$0.006 - 0.001i$	$0.000045i$	0.99	0.85	0.80	$-0.006 - 0.001i$	$-0.08i$
2	4	$0.006 - 0.001i$	$0.000045i$	0.99	0.85	0.80	$-0.006 - 0.001i$	$0.2 - 0.02i$
2	4	$0.006 - 0.001i$	$0.000045i$	0.99	0.85	0.80	$-0.006 - 0.001i$	$-0.3 + 0.02i$
2	4	$0.006 - 0.001i$	$0.000045i$	0.99	0.85	0.80	$-0.006 - 0.001i$	$-0.09 - 0.6i$

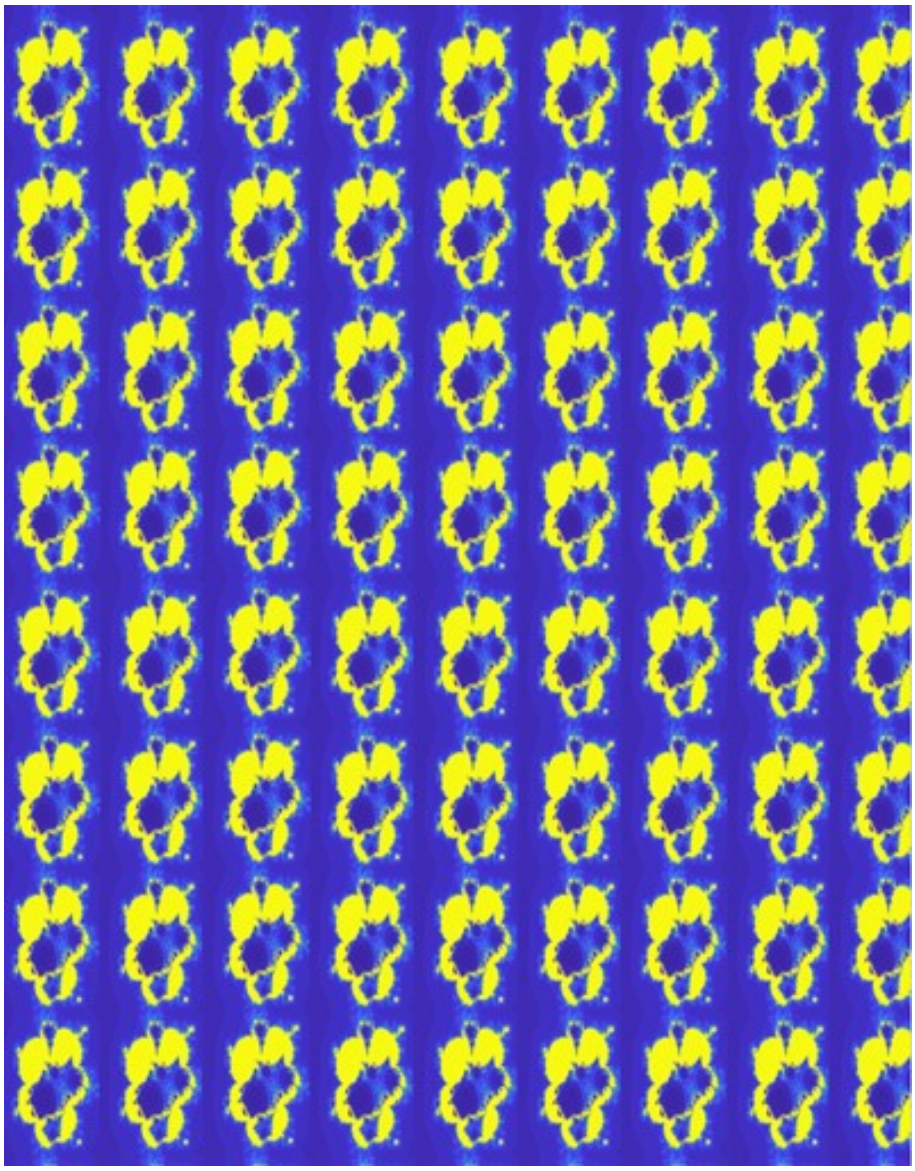

Figure 18: depicts the Batik design obtained by using the third subsection of Figure 17.

Figure 19: depicts the Batik design obtained by using the third subsection of Figure 17.

Comprising repeated Julia sets, Figure 18, shows a Batik fractal pattern with strong visual contrast through vivid yellow areas set against deep blue backgrounds. we use the third section of Figure 17, in which every fractal tile shows uneven but symmetrical patterns marked by dense clusters of brilliant yellow, suggesting areas of fast divergence or escape inside the fractal iteration.

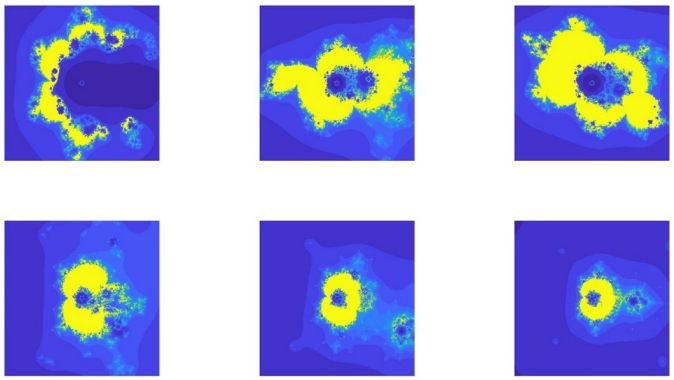

Figure 20: depict the Mandelbrot set fractal for different value of α.

In the first subsection of Figure 20, a fractal with a stretched horizontal structure shows conspicuously in the top row with complex and fragmented edges that clearly highlight fast iterative divergence. Turning toward the second section, the buildings get denser and more centrally arranged; the middle image shows a vivid, symmetric fractal formation defined by two brilliant yellow, lobed clusters merging centrally. The fractal in the third subsection achieves higher complexity by extending into a vivid and irregularly shaped yellow pattern interspersed with smaller intricate blue islands, so indicating more turbulent dynamics. The fractals obviously lose in complexity and spatial coverage in the bottom row from the fourth subsection of this figure, where a brilliant, condensed yellow creation surrounded by fine fractal edges is evident, to the bottom-right subplot, where the fractal form becomes substantially smaller, smoother, and less chaotic.

Table 11: Variation of the parameter α.

n	**m**	**a**	**b**	**s**	**p**	**q**	$\boldsymbol{\alpha}$	$\boldsymbol{\beta}$
2	4	$-1.5+0.1i$	$0.000045i$	0.99	0.85	0.80	-0.09	$-0.0005i$
2	4	$-1.5+0.1i$	$0.000045i$	0.99	0.85	0.80	$-0.5+0.1i$	$-0.0005i$
2	4	$-1.5+0.1i$	$0.000045i$	0.99	0.85	0.80	$-0.3-0.2i$	$-0.0005i$
2	4	$-1.5+0.1i$	$0.000045i$	0.99	0.85	0.80	$0.4+0.05i$	$-0.0005i$
2	4	$-1.5+0.1i$	$0.000045i$	0.99	0.85	0.80	$0.6-0.1i$	$-0.0005i$
2	4	$-1.5+0.1i$	$0.000045i$	0.99	0.85	0.80	0.8	$-0.0005i$

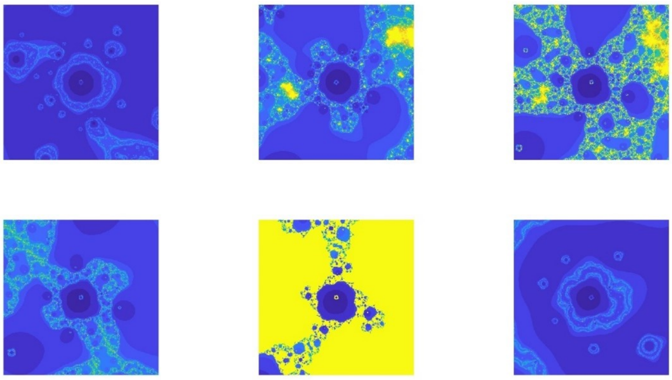

Figure 21: depict the Mandelbrot set fractal for different values of c.

Table 12: Variation of the parameter c.

n	**m**	**a**	**b**	**s**	**p**	**q**	$\boldsymbol{\alpha}$	$\boldsymbol{\beta}$
2	4	$-1.5+0.1i$	$0.000045i$	0.99	0.85	0.80	$-0.006-0.001i$	$-0.05i$
2	4	$-1.5+0.1i$	$0.000045i$	0.99	0.85	0.80	$-0.006-0.001i$	$-0.05i$
2	4	$-1.5+0.1i$	$0.000045i$	0.99	0.85	0.80	$-0.006-0.001i$	$-0.05i$
2	4	$-1.5+0.1i$	$0.000045i$	0.99	0.85	0.80	$-0.006-0.001i$	$-0.05i$
2	4	$-1.5+0.1i$	$0.000045i$	0.99	0.85	0.80	$-0.006-0.001i$	$-0.05i$
2	4	$-1.5+0.1i$	$0.000045i$	0.99	0.85	0.80	$-0.006-0.001i$	$-0.05i$

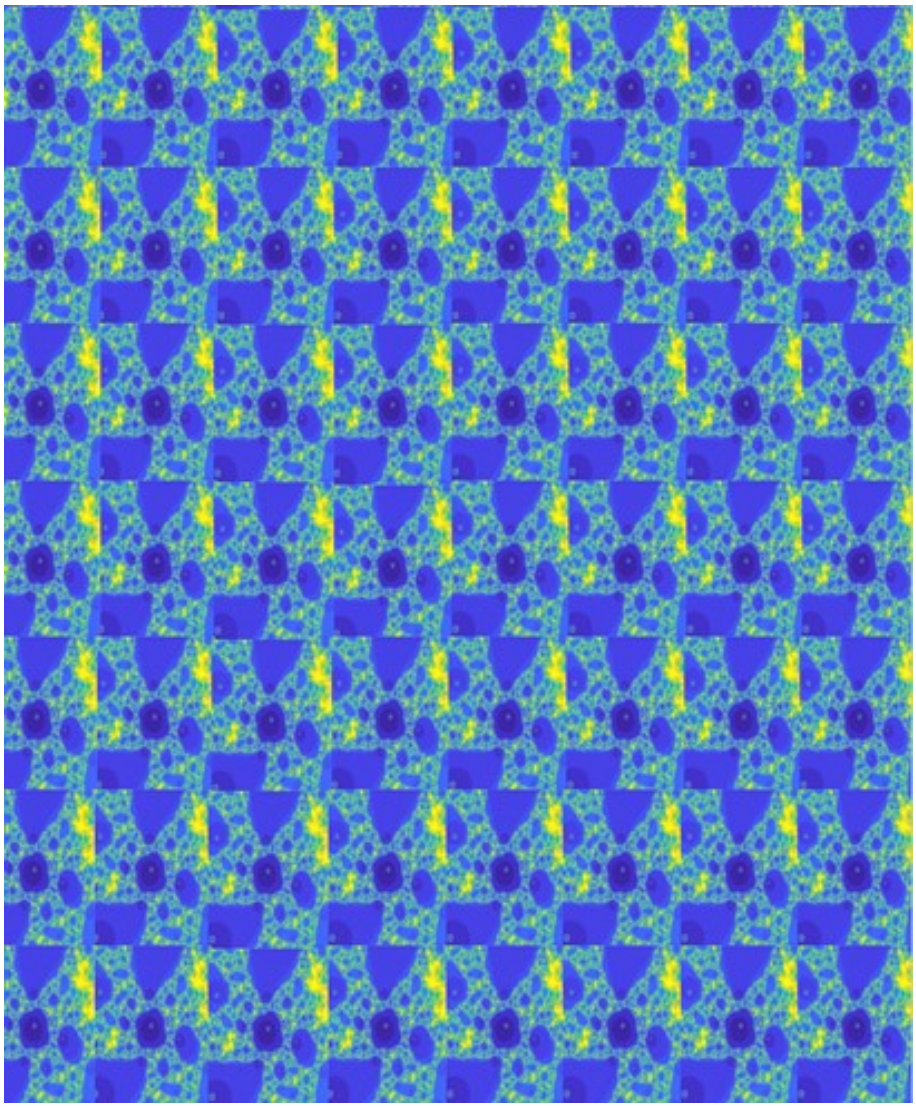

Figure 22: depicts the Batik design obtained by using the third subsection of Figure 21.

Figure 23: depicts the Batik design obtained by using the third subsection of Figure 21.

Figure 22, shows a regular grid that produces a seamless, patterned surface. We use third subsection of Figure 21, the deep blues, brilliant cyan, and vivid yellow hues. Whereas the dark blue areas show more steady, convergent areas of the fractal, the yellow areas indicate zones of fast escape in the iterative process.

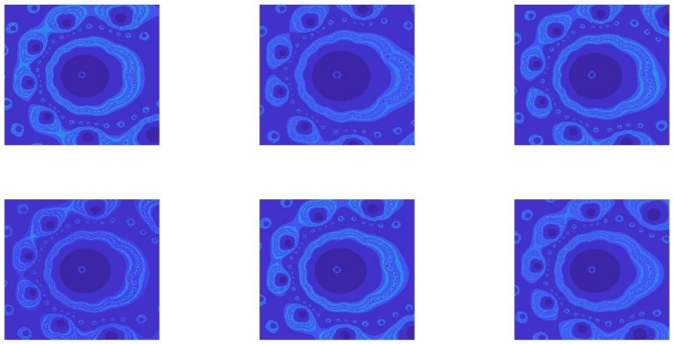

Figure 24: depict the Mandelbrot set fractal for different values of b.

Figure 19 shows the Mandelbrot set fractal structure produced by a generalized viscosity approximation process under various parameter settings, primarily due to changes in the parameter b. Although all subplots share a similar color scheme—mostly dominated by blue and cyan tones—the internal structures exhibit clear variations in shape, complexity, and fractal pattern distribution. The other parameters n, m, a, s, p, q, and α are kept constant. The values of all parameters are listed in Table 13.

Table 13: Variation of the parameter b.

n	**m**	**a**	**b**	**s**	**p**	**q**	$\boldsymbol{\alpha}$	$\boldsymbol{\beta}$
2	5	$-1.5+0.1i$	$0.000045i$	0.99	0.85	0.89	$-0.006-0.001i$	$-0.005i$
2	5	$-1.5+0.1i$	$0.0001+0.00003i$	0.99	0.85	0.89	$-0.006-0.001i$	$-0.005i$
2	5	$-1.5+0.1i$	$-0.00007i$	0.99	0.85	0.89	$-0.006-0.001i$	$-0.005i$
2	5	$-1.5+0.1i$	$0.00003-0.00005i$	0.99	0.85	0.89	$-0.006-0.001i$	$-0.005i$
2	5	$-1.5+0.1i$	$0.00002+0.00006i$	0.99	0.85	0.89	$-0.006-0.001i$	$-0.005i$
2	5	$-1.5+0.1i$	$-0.00005-0.00002i$	0.99	0.85	0.89	$-0.006-0.001i$	$-0.005i$

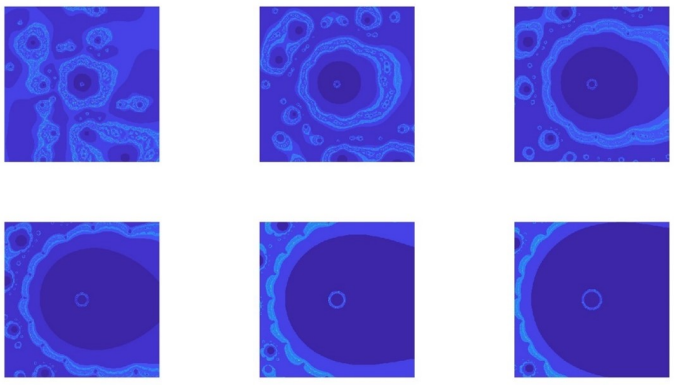

Figure 25: depict the Mandelbrot set fractal for different values m.

In Figure 25, shows the variation in Mandelbrot set fractal with different values of m

while other parameters are fixed. The values are shown in Table 14.

Table 14: Variation of the parameter m.

n	**m**	**a**	**b**	**s**	**p**	**q**	$\boldsymbol{\alpha}$	$\boldsymbol{\beta}$
2	3	$-1.5+0.1i$	$0.000045i$	0.99	0.85	0.89	$-0.0006-0.001i$	$0.005i$
2	4	$-1.5+0.1i$	$0.000045i$	0.99	0.85	0.89	$-0.0006-0.001i$	$0.005i$
2	5	$-1.5+0.1i$	$0.000045i$	0.99	0.85	0.89	$-0.0006-0.001i$	$0.005i$
2	6	$-1.5+0.1i$	$0.000045i$	0.99	0.85	0.89	$-0.0006-0.001i$	$0.005i$
2	7	$-1.5+0.1i$	$0.000045i$	0.99	0.85	0.89	$-0.0006-0.001i$	$0.005i$
2	8	$-1.5+0.1i$	$0.000045i$	0.99	0.85	0.89	$-0.0006-0.001i$	$0.005i$

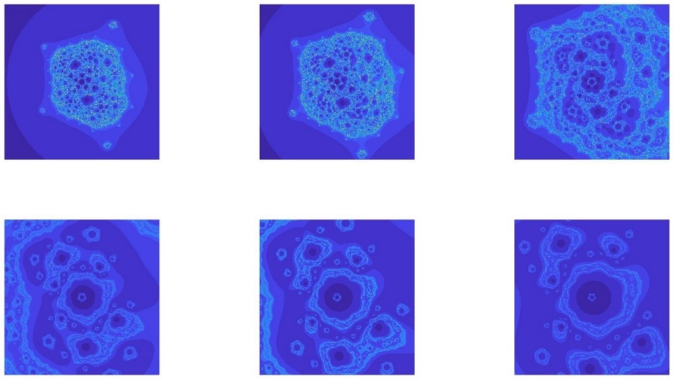

Figure 26: depict the Mandelbrot set fractal for different values m.

Figure 26 shows the behavior of the Mandelbrot set fractals generated using the generalized viscosity approximation process with variation in the parameter b, while the other parameters n, m, a, s, p, q, α, and β are kept fixed.

Table 15: Variation of the parameter p.

n	**m**	**a**	**b**	**s**	**p**	**q**	$\boldsymbol{\alpha}$	$\boldsymbol{\beta}$
2	4	$-1.5+0.1i$	$0.00045i$	0.99	0.20	0.89	$-0.0006-0.001i$	$-0.005i$
2	4	$-1.5+0.1i$	$0.00045i$	0.99	0.30	0.89	$-0.0006-0.001i$	$-0.005i$
2	4	$-1.5+0.1i$	$0.00045i$	0.99	0.50	0.89	$-0.0006-0.001i$	$-0.005i$
2	4	$-1.5+0.1i$	$0.00045i$	0.99	0.70	0.89	$-0.0006-0.001i$	$-0.005i$
2	4	$-1.5+0.1i$	$0.00045i$	0.99	0.75	0.89	$-0.0006-0.001i$	$-0.005i$
2	4	$-1.5+0.1i$	$0.00045i$	0.99	0.80	0.89	$-0.0006-0.001i$	$-0.005i$

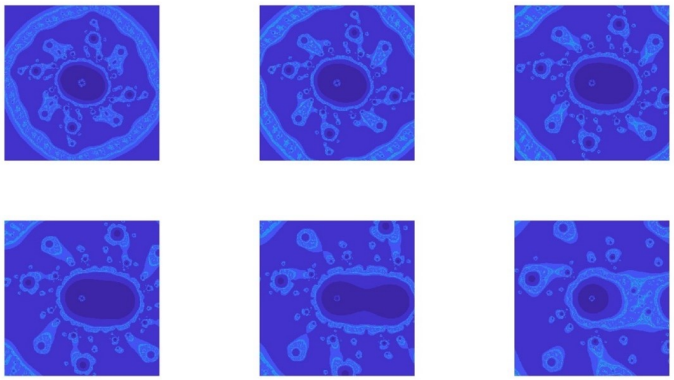

Figure 27: depict the Mandelbrot set fractal for different values of q.

In Figure 27, the Mandelbrot set fractals in first three subsections shows rather high radial symmetry. Top-left, the first subsection of this figure shows a nearly circular central structure encased in a large outer ring with symmetrical appendages spreading out like petals. Moving rightward, these structures stretch horizontally especially in the top-center and top-right plots, where the central shape develops into an oval or ellipsis, and the radiating patterns elongate and slightly change to produce a dynamic flow suggestive of motion. The bottom row carries on this change toward ever more asymmetry and complexity. The radiating arms stay but are more irregular and scattered while the central oval gets bigger and more stretched. Strong horizontal axis of symmetry is shown in the bottom-left and bottom-center images; the fractal forms an eye-like or capsule form there. With denser internal patterns and asymmetrically distributed mini-islands, the structure morphs into a more abstract form akin to a biological or cellular geometry by the bottom-right image.

Table 16: Variation of the parameter q.

n	**m**	**a**	**b**	**s**	**p**	**q**	$\boldsymbol{\alpha}$	$\boldsymbol{\beta}$
2	4	$-1.5+0.1i$	$0.000045i$	0.99	0.85	0.10	$-0.006-0.001i$	$-0.005i$
2	4	$-1.5+0.1i$	$0.000045i$	0.99	0.85	0.30	$-0.006-0.001i$	$-0.005i$
2	4	$-1.5+0.1i$	$0.000045i$	0.99	0.85	0.50	$-0.006-0.001i$	$-0.005i$
2	4	$-1.5+0.1i$	$0.000045i$	0.99	0.85	0.60	$-0.006-0.001i$	$-0.005i$
2	4	$-1.5+0.1i$	$0.000045i$	0.99	0.85	0.70	$-0.006-0.001i$	$-0.005i$
2	4	$-1.5+0.1i$	$0.000045i$	0.99	0.85	0.80	$-0.006-0.001i$	$-0.005i$

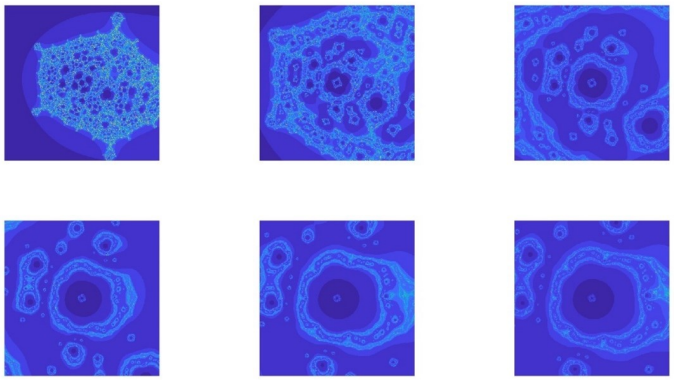

Figure 28: depict the Mandelbrot set fractal for different values of s.

Figure 28 shows the Mandelbrot set fractal structure produced by a generalized viscosity approximation process under various parameter settings, primarily due to changes in the parameter s. The other parameters n, m, a, b, p, q, and α are kept constant. The values of all parameters are listed in Table 17.

Table 17: Variation of the parameter s.

n	**m**	**a**	**b**	**s**	**p**	**q**	$\boldsymbol{\alpha}$	$\boldsymbol{\beta}$
2	3	$-1.5+0.1i$	$0.0045i$	0.20	0.85	0.89	$-0.006-0.001i$	$-0.005i$
2	3	$-1.5+0.1i$	$0.0045i$	0.40	0.85	0.89	$-0.006-0.001i$	$-0.005i$
2	3	$-1.5+0.1i$	$0.0045i$	0.60	0.85	0.89	$-0.006-0.001i$	$-0.005i$
2	3	$-1.5+0.1i$	$0.0045i$	0.80	0.85	0.89	$-0.006-0.001i$	$-0.005i$
2	3	$-1.5+0.1i$	$0.0045i$	0.95	0.85	0.89	$-0.006-0.001i$	$-0.005i$
2	3	$-1.5+0.1i$	$0.0045i$	0.99	0.85	0.89	$-0.006-0.001i$	$-0.005i$

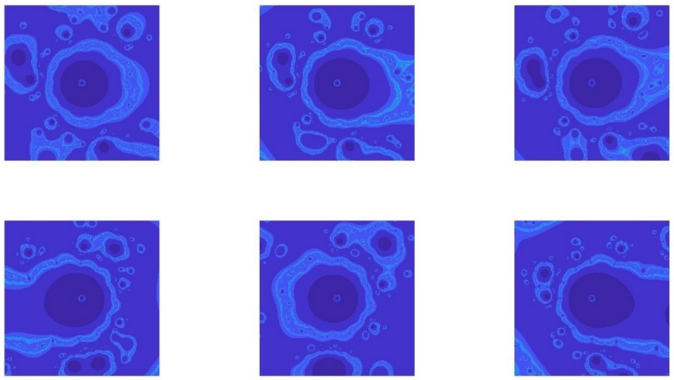

Figure 29: depict the Mandelbrot set fractal for different values of a.

Figure 29 shows the Mandelbrot set fractal structure produced by a generalized viscosity approximation process under various parameter settings, primarily due to changes in the parameter a. The other parameters n, m, s, b, p, q, and α are kept constant. The values of all parameters are listed in Table 18.

Table 18: Variation of the parameter a.

n	**m**	**a**	**b**	**s**	**p**	**q**	$\boldsymbol{\alpha}$	$\boldsymbol{\beta}$
2	5	$-1.5+0.1i$	$0.000045i$	0.99	0.85	0.89	$-0.006-0.001i$	$-0.005i$
2	5	$-2+0.2i$	$0.000045i$	0.99	0.85	0.89	$-0.006-0.001i$	$-0.005i$
2	5	$-1.8-0.3i$	$0.000045i$	0.99	0.85	0.89	$-0.006-0.001i$	$-0.005i$
2	5	$2.2+0.4i$	$0.000045i$	0.99	0.85	0.89	$-0.006-0.001i$	$-0.005i$
2	5	$1.6-0.2i$	$0.000045i$	0.99	0.85	0.89	$-0.006-0.001i$	$-0.005i$
2	5	$-2.5+0.5i$	$0.000045i$	0.99	0.85	0.89	$-0.006-0.001i$	$-0.005i$

4. Comparative Analysis

In this section, we compare our work with Rawat et al. [18], Tanveer et al. [19], Kumari et al. [21], and Kumari et al. [24].

Table 19: Comparative analysis of the proposed work with existing studies.

Aspect / Study	**Rawat et al. (2024)**	**Tanveer et al. (2023)**	**Kumari et al. (2022)**	**Kumari et al. (2024)**	**Our Paper**
Iterative Scheme Used	SP-iteration	Mann, Picard–Mann	Viscosity Approximation	Viscosity Approximation	Viscosity + s-Convexity
Mapping Type	Generalized Rational	Transcendental (log)	Nonlinear/Polynomial	Nonlinear	Generalized Rational-Type
s-Convexity Usage	Yes	No	No	No	Yes
Graphical Implementation	Yes	Yes	Yes	Yes	Yes
Parameter Sensitivity Study	Moderate	Moderate	Extensive	Extensive	Highly Detailed with Design Impact
Visual Application	Fractal Visualization Only	Fractal Structure Study	Includes Biomorphs	Structural Focus	Batik Textile Design

5. Conclusions

This work has investigated the use of a generalized viscosity approximation-type iteration with s-convexity for the generation and visualization of Julia and Mandelbrot sets derived from a generalized rational-type complex polynomial. Generating exact and meaningful fractal images depends largely on the introduction of a custom escape criterion, which ensures accurate orbit classification. We have successfully demonstrated how variations in iteration parameters significantly influence the geometry, complexity, and connectivity of both Julia and Mandelbrot fractals. Moreover, their potential applications in textile design have been explored. By bridging complex dynamics with computational aesthetics, the results connect theoretical mathematical constructions with practical creative applications. In future work, we intend to explore new iterative techniques for quaternion-based extensions to three-dimensional fractals. These more complex volumetric structures revealed by Julia sets could prove highly valuable for 3D printing of fractal sculptures or modeling of physical phenomena.

Acknowledgements

The authors extend their gratitude to the Deanship of Graduate Studies and Scientific Research of the Islamic University of Madinah for the support provided to the Post Publication Program 4.

Author Contribution: All authors contributed equally.
Conflict of Interest: The authors declare no conflict of interest.
Data Availability Statement: No dataset was used in this study.

References

[1] A. Husain, M. N. Nanda, M. S. Chowdary, and M. Sajid. Fractals: An eclectic survey, part-i. *Fractal and Fractional*, 6:89, 2022.

[2] A. Husain, M. N. Nanda, M. S. Chowdary, and M. Sajid. Fractals: An eclectic survey, part ii. *Fractal and Fractional*, 6:379, 2022.

[3] G. Julia. Mémoire sur l'itération des fonctions rationnelles. *Journal de Mathématiques Pures et Appliquées*, 1:47–245, 1918.

[4] P. Fatou. Sur les substitutions rationnelles. *Comptes Rendus Hebdomadaires des Séances de l'Académie des Sciences*, 164:806–808, 1917.

[5] B. Mandelbrot. *The Fractal Geometry of Nature*. W. H. Freeman, San Francisco, 1982.

[6] W. Mann. Mean value methods in iteration. *Proceedings of the American Mathematical Society*, 4:506–510, 1953.

[7] B. Halpern. Fixed points of nonexpanding maps. *Bulletin of the American Mathematical Society*, 73:957–961, 1967.

[8] A. Moudafi. Viscosity approximation methods for fixed-points problems. *Journal of Mathematical Analysis and Applications*, 241:46–55, 2000.

[9] P. Mainge. The viscosity approximation process for quasi-nonexpansive mappings in hilbert spaces. *Computers & Mathematics with Applications*, 59:74–79, 2010.

[10] M. Romera, G. Pastor, G. Alvarez, and F. Montoya. Growth in complex exponential dynamics. *Computers & Graphics*, 24:143–151, 2000.

[11] M. Abbas, H. Iqbal, and M. De la Sen. Generation of julia and mandelbrot sets via fixed points. *Symmetry*, 12:86, 2020.

[12] L. K. Mork and D. J. Ulness. Visualization of mandelbrot and julia sets of möbius transformations. *Fractal and Fractional*, 5:73, 2021.

[13] H. Qi, M. Tanveer, W. Nazeer, and Y. Chu. Fixed point results for fractal generation of complex polynomials involving sine function via non-standard iterations. *IEEE Access*, 8:154301–154317, 2020.

[14] N. Hamada and F. Kharbat. Mandelbrot and julia sets of complex polynomials involving sine and cosine functions via picard–mann orbit. *Complex Analysis and Operator Theory*, 17:13, 2023.

[15] D. J. Prajapati, S. Rawat, A. Tomar, M. Sajid, and R. C. Dimri. A brief study on julia sets in the dynamics of entire transcendental function using mann iterative scheme. *Fractal and Fractional*, 6:397, 2022.

[16] A. Tomar, V. Kumar, U. S. Rana, and M. Sajid. Fractals as julia and mandelbrot sets of complex cosine functions via fixed point iterations. *Symmetry*, 15:478, 2023.

[17] M. R. Pinheiro. s-convexity–foundations for analysis. *Differential Geometry - Dynamical Systems*, 10:257–262, 2008.

[18] S. Rawat, D. J. Prajapati, A. Tomar, and K. Gdawiec. Generation of mandelbrot and julia sets for generalized rational maps using sp-iteration process equipped with s-convexity. *Mathematics and Computers in Simulation*, 220:148–169, 2024.

[19] M. Tanveer, W. Nazeer, and K. Gdawiec. On the mandelbrot set of $z^p + \log c$ via

the mann and picard–mann iterations. *Mathematics and Computers in Simulation*, 209:184–204, 2023.

[20] A. Tassaddiq. General escape criteria for the generation of fractals in extended jungck–noor orbit. *Mathematics and Computers in Simulation*, 196:1–14, 2022.

[21] S. Kumari, K. Gdawiec, A. Nandal, M. Postolache, and R. Chugh. A novel approach to generate mandelbrot sets, julia sets and biomorphs via viscosity approximation method. *Chaos, Solitons & Fractals*, 163:112540, 2022.

[22] S. Kumari, M. Kumari, and R. Chugh. Dynamics of superior fractals via jungck sp orbit with s-convexity. *Analele Universitatii din Craiova, Seria Matematica Informatica*, 46:344–365, 2019.

[23] A. Nandal, R. Chugh, and M. Postolache. Iteration process for fixed point problems and zeros of maximal monotone operators. *Symmetry*, 11:655, 2019.

[24] S. Kumari, K. Gdawiec, A. Nandal, N. Kumar, and R. Chugh. On the viscosity approximation type iterative method and its non-linear behavior in the generation of mandelbrot and julia sets. *Numerical Algorithms*, 96:211–236, 2024.

[25] R. L. Devaney. *A First Course in Chaotic Dynamical Systems: Theory and Experiment*. CRC Press, Boca Raton, 1 edition, 2018.

[26] H. O. Peitgen, H. Jürgens, and D. Saupe. *Chaos and Fractals: New Frontiers of Science*. Springer, New York, 2004.

[27] İ. Araz and M. A. Çetin. Fractal-fractional modeling of the covid-19 spread with deterministic and stochastic approaches. *International Journal of Applied and Computational Mathematics*, 11(1):4, 2025.

[28] S. İ. Araz. New class of volterra integro-differential equations with fractal-fractional operators: Existence, uniqueness and numerical scheme. *Discrete and Continuous Dynamical Systems - Series S*, 14(7), 2021.

[29] T. Mekkaoui, A. Atangana, and S. İ. Araz. Predictor–corrector for non-linear differential and integral equation with fractal–fractional operators. *Engineering with Computers*, 37(3):2359–2368, 2021.

[30] F. Uddin, U. Ishtiaq, N. Saleem, K. Ahmad, and F. Jarad. Fixed point theorems for controlled neutrosophic metric-like spaces.

[31] U. Ishtiaq, D. A. Kattan, K. Ahmad, T. A. Lazăr, V. L. Lazăr, and L. Guran. On intuitionistic fuzzy n_b metric space and related fixed point results with application. *Fractal and Fractional*, 7(7):529, 2023.

[32] U. Ishtiaq, M. Asif, A. Hussain, K. Ahmad, I. Saleem, and H. Al Sulami. Extension of a unique solution in generalized neutrosophic cone metric spaces. *Symmetry*, 15(1):94, 2022.